

Panoscopic non-equilibrium fluctuation identity

Juliana Caspers,^{1,*} Karthika Krishna Kumar,² Clemens Bechinger,² and Matthias Krüger^{1,†}

¹*Institute for Theoretical Physics, Georg-August-Universität Göttingen, 37073 Göttingen, Germany*

²*Fachbereich Physik, Universität Konstanz, 78457 Konstanz, Germany*

Quantifying and characterizing fluctuations far away from equilibrium is a challenging task. We introduce and experimentally confirm an identity for a driven classical system, relating the different non-equilibrium cumulants of the observable conjugate to the driving protocol. The identity is valid from micro- to macroscopic length scales, and it encompasses the fluctuation dissipation theorem. We apply it in experiments of a Brownian probe particle confined and driven by an optical potential and suspended in a nonlinear and non-Markovian fluid.

The fluctuation dissipation theorem [1, 2], connecting response and fluctuations of equilibrium systems, is of fundamental importance for condensed matter, fluids, plasmas, or electromagnetic fields [3–6]. One of its remarkable properties is the validity at any length scale, be it the nanoscale, as for electric charges, or the macroscale, as for the macroscopic magnetization. It is however restricted to the linear regime, i.e., to situations close to equilibrium. Most previous research has been largely devoted to determining similar relations for non-equilibrium steady states [7–29] as well as for nonlinear responses [30–47]. A typical observation in the found relations is the explicit appearance of microscopic details – sometimes referred to as frenetic components [48, 49] – often hampering a model independent formulation as well as systematic change of length scales such as coarse graining to macroscopic scales [42, 43, 45]. As a consequence, experimental test and application of such relations has indeed been successful for systems with a small number of accessible Markovian degrees of freedom [47, 50–53].

In this letter, we introduce and experimentally confirm an identity for a driven classical system which relates the different non-equilibrium cumulants of the observable conjugate to the driving protocol, up to a certain order in driving velocity. We demonstrate that (i) this identity is valid from micro- to macroscopic length scales, (ii) that it is model independent, and (iii) that it encompasses the fluctuation dissipation theorem. We apply it in an experimental many body system of a Brownian probe particle interacting with worm-like micelles and confined and driven by an optical potential. In these experiments, we demonstrate that the third force cumulant quantifies the deviation from the fluctuation dissipation theorem in second order in driving. Notably, our theoretical predictions demonstrate that the form of the FDT remains valid for purely Gaussian observables within the displayed order.

Consider a classical system of stochastic degrees \mathbf{x}_t at time t , (weakly) coupled to a heat bath at temperature T . The system’s potential energy U depends on \mathbf{x}_t and on a time dependent deterministic protocol X_t , i.e., $U(\mathbf{x}_t, X_t)$. The system is prepared in equilibrium at time $t \rightarrow -\infty$, with protocol value $X_{-\infty} = X_t$, for simplicity [54]. The time dependence of the protocol drives the system away

from equilibrium.

The derivative of U with respect to X_t , $F_t := \partial_{X_t} U(\mathbf{x}_t, X_t)$ is the observable conjugate to X_t . E.g., if X_t is a position as in our experiments, F_t is (minus) the corresponding force. F_t can be micro- or macroscopic; for example, let X couple linearly to an observable $A(\mathbf{x})$, $U(\mathbf{x}_t, X_t) = U(\mathbf{x}_t, 0) - X_t A(\mathbf{x}_t)$, i.e., $F_t = -A(\mathbf{x}_t)$. Thus, if $A(\mathbf{x})$ is a macroscopic field, such as the macroscopic magnetization, F_t is macroscopic. If $A(\mathbf{x})$ is the position of a molecular particle, F_t is microscopic. The following remains valid if X_t enters U nonlinearly.

The statistical properties of F_t in this non-equilibrium situation are encoded in its cumulants and its correlations with another state observable $B_t = B(\mathbf{x}_t, X_t)$, which we aim to study here. The well known fluctuation dissipation theorem (FDT) connects the covariance in the unperturbed system and the first moment of B under weak driving [1, 2],

$$\beta^2 \int_{-\infty}^t ds \dot{X}_s \langle B_t; F_s \rangle_{\text{eq}} = \beta [\langle B_t \rangle - \langle B_t \rangle_{\text{eq}}] + \mathcal{O}(\dot{X}^2), \quad (1)$$

with $\beta = 1/k_B T$ and Boltzmann constant k_B . $\langle \dots; \dots \rangle$ denotes the 2nd cumulant, and similarly for higher orders below.

In an accompanying manuscript [54] we derive identities connecting the non-equilibrium cumulants of F_t and B_t to different orders. These give rise to the following series involving the mentioned cumulants [54],

$$\begin{aligned} \beta^2 \int_{-\infty}^t ds \dot{X}_s \langle B_t; F_s \rangle &= \beta [\langle B_t \rangle - \langle B_t \rangle_{\text{eq}}] \\ &+ \frac{\beta^3}{2} \int_{-\infty}^t ds \int_{-\infty}^t ds' \dot{X}_s \dot{X}_{s'} \langle B_t; F_s; F_{s'} \rangle \\ &- \frac{\beta^4}{6} \int_{-\infty}^t ds \int_{-\infty}^t ds' \int_{-\infty}^t ds'' \dot{X}_s \dot{X}_{s'} \dot{X}_{s''} \\ &\times \langle B_t; F_s; F_{s'}; F_{s''} \rangle + \mathcal{O}(\dot{X}^4), \end{aligned} \quad (2)$$

Eq. (2) is, as indicated, correct up to fourth order in driving \dot{X}_t under the assumption of local detailed balance [55, 56]. Expanding Eq. (2) to first order yields FDT in Eq. (1), so that it is included in Eq. (2). To

higher orders, first and second cumulants do not fulfill FDT, and Eq. (2) quantifies their difference in terms of third and fourth cumulants of F and B . Notably, the second to fourth lines of Eq. (2) vanish for purely Gaussian distributed F and B , so that first and second cumulants obey FDT to the given non-equilibrium order. While Eq. (2) suggests a continuation with higher order terms [54], we have derived it to the order given in Eq. (2). It is important to note that in Eq. (2) the protocol \hat{X} appears as prefactors as well as in the non-equilibrium cumulants themselves.

We exploit Eq. (2) with experiments of Brownian particles interacting with micellar fluid. Specifically, we use silica particles of diameter $\sim 1 \mu\text{m}$ suspended in a 5 mM equimolar solution of cetylpyridinium chloride monohydrate (CPyCl) and sodium salicylate (NaSal). At concentrations above the critical micellar concentration ($\gtrsim 4 \text{ mM}$), this fluid is known to form giant worm-like micelles leading to a viscoelastic nonlinear behavior at ambient temperatures [57], see SM. At 5 mM, we determine the relaxation time of the fluid from microrheological recoil experiments to be $\sim 3 \text{ s}$ [58]. A small amount of silica particles is added to the micellar solution which is contained in a rectangular capillary with $100 \mu\text{m}$ height and kept at a temperature of 25°C . This sample is placed on a custom-built optical tweezer setup that uses a Gaussian laser beam of wavelength 532 nm and a $100\times$ oil immersion objective ($\text{NA} = 1.45$). The laser beam yields a potential $U(x_t - X_t)$ as shown in Fig. 1(a), centered at X_t , trapping one of the silica particles with coordinate x_t . $F_t = \partial_{x_t} U(x_t - X_t)$ is thus the force acting on the particle by the trapping potential (or vice versa). As the micellar degrees do not couple to X , they do not enter F_t explicitly, and how they enter U is not important. We consider $B \equiv F$, and made the potential asymmetric, to obtain a finite second order response of $\beta\langle F_t \rangle$. This allows to test Eq. (2) to second order in our experiments, and it is achieved by a controlled lateral displacement of the vertically incident laser beam from the center of the objective lens (see SM).

To apply the driving protocol, the sample cell is moved, while the optical trap remains stationary in our experiments. This is achieved using a piezo-driven stage on which the sample is mounted and translated in an oscillating manner relative to the trap. In the fluid's rest frame, this yields a periodic motion of the potential minimum X_t , i.e., the protocol,

$$X_t = \hat{X} \sin(\omega t), \quad (3)$$

with amplitude \hat{X} and frequency ω . Particle trajectories are recorded with a frame rate of $\sim 150 \text{ Hz}$ using a video camera and particle positions are determined using a custom MATLAB algorithm. To yield sufficient statistics, each protocol (\hat{X}, ω) was measured over 1400s. We allowed the system to reach a steady state by recording trajectories only after at least 5 oscillation periods

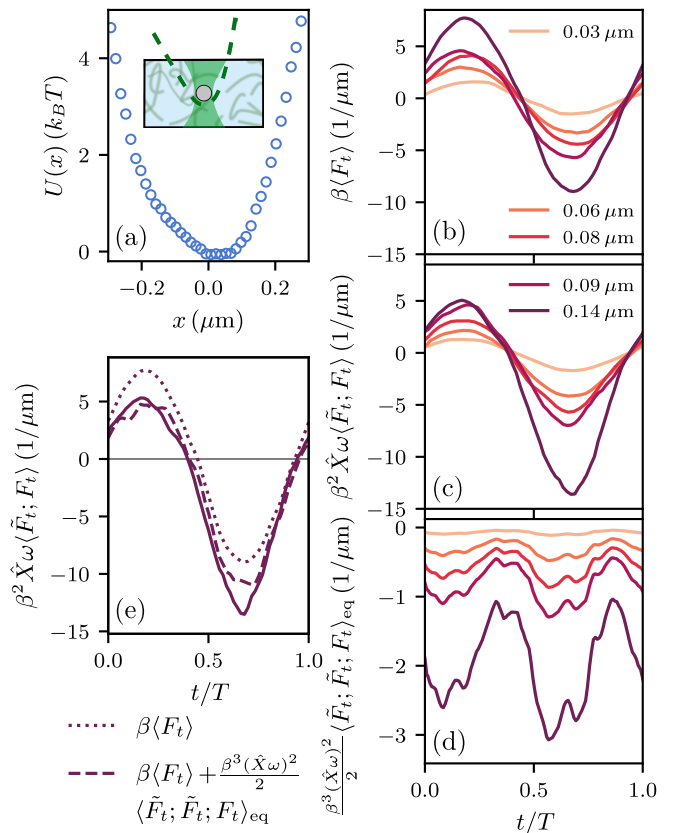


FIG. 1. (a) Asymmetric optical potential $U(x) = -k_B T \ln P(x)$ felt by the probe particle (inset sketch), with $P(x)$ the probability distribution with the trap at rest. (b) Mean force $\beta\langle F_t \rangle$, (c) force covariance $\beta^2 \hat{X} \omega \langle \tilde{F}_t; F_t \rangle$, and (d) third cumulant $\beta^2 (\hat{X} \omega)^2 \langle \tilde{F}_t; \tilde{F}_t; F_t \rangle_{\text{eq}} / 2$, as functions of time, for driving frequency $\omega = 8.4 \text{ rad/s}$ and amplitudes $\hat{X} = \{0.03, 0.06, 0.08, 0.09, 0.14\} \mu\text{m}$ as labeled. $T = \frac{2\pi}{\omega}$. (e) Force covariance (solid line), mean force (dotted line), and sum of mean force and third force cumulant (dashed line, Eq. (4)) for $\hat{X} = 0.14 \mu\text{m}$.

have passed. Prior to each non-equilibrium protocol, we recorded particle trajectories for another 1000s with X_t at rest. This equilibrium data were used to check that the form of U does not vary between measurements, and also to obtain the force cumulants under equilibrium conditions.

With the protocol of Eq. (3), Eq. (2) takes the form

$$\beta^2 \hat{X} \omega \langle \tilde{F}_t; F_t \rangle = \beta \langle F_t \rangle + \frac{\beta^3 \hat{X}^2 \omega^2}{2} \langle \tilde{F}_t; \tilde{F}_t; F_t \rangle_{\text{eq}} + \mathcal{O}((\hat{X} \omega)^3), \quad (4)$$

where the tilde denotes cosine transform, i.e., $\tilde{F}_t \equiv \int_{-\infty}^t ds \cos(\omega s) F_s$. We restrict the analysis to the lowest nontrivial, i.e., second, order and expanded Eq. (2) accordingly, also using $\langle F_t \rangle_{\text{eq}} = 0$. The cumulants in Eq. (4) depend on time t in a periodic manner, as shown in Figs. 1(b)-(d), for $\omega = 8.4 \text{ rad/s}$ [59] and driving ampli-

tudes ranging from $\hat{X} = 0.03 \mu\text{m}$ (light) to $\hat{X} = 0.14 \mu\text{m}$ (dark). Fig. 1(b) shows the mean force, which, as expected for a driven oscillator, is a periodic function with period $T = \frac{2\pi}{\omega}$. For the smallest amplitude shown, the mean force is nearly harmonic with frequency ω , as expected from linear response. With growing amplitude, higher harmonics occur, as expected from nonlinear response. This asymmetric system shows second order response with frequencies of 2ω and 0ω .

Fig. 1(c) shows the force covariance for the same parameters and color code. For small amplitude \hat{X} , the curves in Figs. 1(b) and (c) are equal within experimental accuracy, as analyzed in detail below. For larger driving amplitude, the force covariance develops higher harmonics with signatures of second order. Very little is known about the properties of such non-equilibrium fluctuations, and quantifying these is difficult. It is notable that the curves in Fig. 1(c), for larger amplitudes, deviate from Fig. 1(b), the deviation which we claim to be quantified by Eq. (4).

Fig. 1(d) shows the third cumulant of force for the same parameters and color code. We have here restricted to the equilibrium cumulant as it appears in Eq. (4), multiplied by $(\hat{X}\omega)^2$. The curves in Fig. 1(d) thus differ only because of the factor $(\hat{X}\omega)^2$. They thus scale quadratically in driving velocity and only show frequencies of 2ω and 0ω .

Eq. (4) states that, in the shown range of amplitudes, the curves in Fig. 1(c) are given by the sum of the curves in Figs. 1(b) and (d). For $\hat{X} = 0.14 \mu\text{m}$ the respective summed curve is shown as a dashed line together with the mean force and the force covariance in Fig. 1(e). The agreement is convincing and a confirmation of Eq. (4).

To test this prediction systematically, we dissect the curves in Figs. 1 (b), (c) and (d) into the contributions from harmonics with frequencies 0ω , ω , and 2ω , respectively, i.e., we expand the cumulant of order n into harmonics with frequency $m\omega$,

$$\beta^n (\hat{X}\omega)^{n-1} \langle (\tilde{F}_t)^{n-1} F_t \rangle = \sum_{m=0}^{\infty} A_m^{(n)} \sin(m\omega t + \phi_m^{(n)}), \quad (5)$$

where the coefficients $A_m^{(n)}$ depend on $\hat{X}\omega$. We set $\phi_0^{(n)} \equiv \pi/2$ for consistency. Eq. (4), projected on the harmonic of order m , yields relations between coefficients and phases for each m , which we can test.

Fig. 2 shows the coefficients $A_m^{(n)}$ as a function of driving amplitude \hat{X} . The top panel gives the order $m = 1$, which is seen to be linear in \hat{X} for the range shown, as expected from linear response. The graph shows the mean force (data points) as well as the force covariance (line), the latter evaluated from equilibrium trajectories. Non-equilibrium contributions to the covariance are small for $m = 1$ and the shown range of \hat{X} . The agreement in

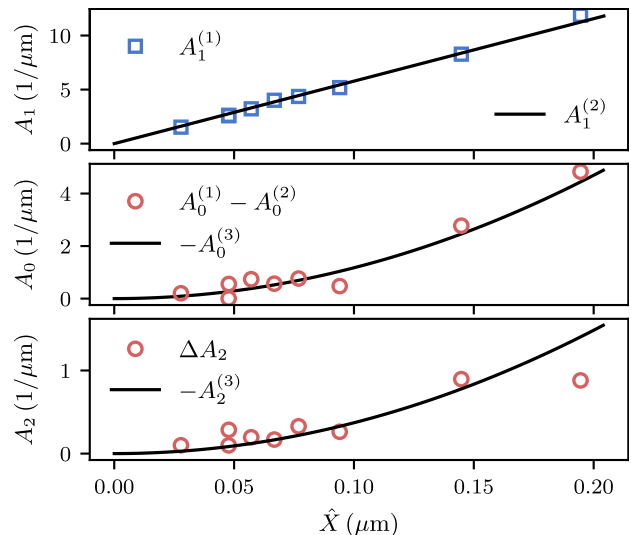


FIG. 2. Coefficients A_m corresponding to harmonics with frequency $m\omega$, as a function of driving amplitude \hat{X} , for $\omega = 8.4 \text{ rad/s}$. Top panel: $m = 1$, demonstrating FDT. Lower panels: Difference of first and second cumulants (data points), and third cumulant (lines) for $m = 0$ and $m = 2$. The agreement confirms Eq. (4). $\Delta A_2 \equiv [(A_2^{(1)})^2 + (A_2^{(2)})^2 - 2A_2^{(1)}A_2^{(2)} \cos(\phi_2^{(1)} - \phi_2^{(2)})]^{1/2}$ [60].

this panel is expected from the fluctuation dissipation theorem.

The center and lower panels in Fig. 2 show the orders $m = 0$ and $m = 2$, respectively. Specifically, these panels present the difference of first and second cumulants in Eq. (4) (data points), i.e., $\beta \langle F_t \rangle - \beta^2 \hat{X}\omega \langle \tilde{F}_t; F_t \rangle_2$, together with the third cumulant (line), $-\beta^3 (\hat{X}\omega)^2 \langle \tilde{F}_t; F_t; F_t \rangle_{\text{eq}}/2$ [60]. The latter is shown as a parabola with curvature obtained from the third force cumulant at equilibrium. The data points in this graph thus quantify the deviation from FDT, with the line giving the prediction of Eq. (4) for this deviation. The agreement is convincing for both $m = 0$ and $m = 2$, supporting the validity of Eq. (4).

As the data in the top panel of Fig. 2 grow linearly and the ones in the center and lower panels grow quadratically with \hat{X} , we fit a line and a parabola to obtain the respective slope and curvature for each m . The obtained values – divided by the respective power in ω – are shown in Fig. 3 as a function of frequency ω . We observe convincing agreement for the measured frequencies further supporting Eq. (4). In tendency, the coefficients decrease with increasing ω , as expected for an overdamped system. Notably, the statistical accuracy of the data points decreases with decreasing ω ; With smaller ω , longer trajectories are required as the period of the cosine transform increases.

Fig. 4 provides the final test of Eq. (4), namely the phases $\phi_m^{(n)}$ of Eq. (5). These hardly depend on driving amplitude and the shown data are averaged over the measured values of \hat{X} . The top panel of Fig. 4 shows

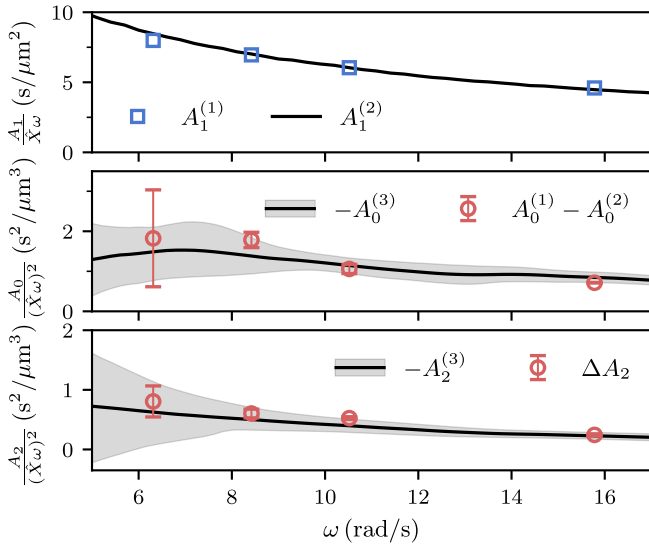


FIG. 3. Coefficients A_m , normalized as labeled, as a function of frequency ω . The agreement in the top panel confirms FDT, the agreement in the lower panels confirms Eq. (4). Each data point is obtained from averaging over driving amplitudes taking the respective scaling of A_m with \hat{X} into account (see SM). Error bars are obtained from partitioning trajectories into two pieces (data points) and from the standard deviation between separate series of measurements (grey area).

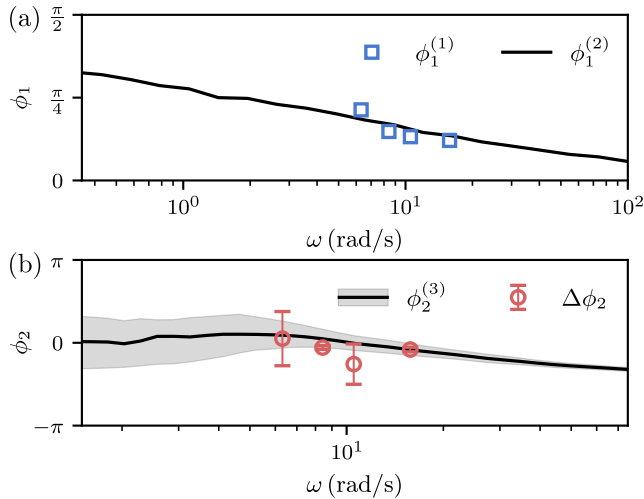


FIG. 4. Phase angles ϕ_1 and ϕ_2 of the harmonics in Eq. (5), as functions of ω . Top panel shows phases of linear response. Lower panel shows the phase of second order response, comparing the contributions of the terms in Eq. (4). $\Delta\phi_2 \equiv \arctan \frac{A_2^{(1)} \sin \phi_2^{(1)} - A_2^{(2)} \sin \phi_2^{(2)}}{A_2^{(1)} \cos \phi_2^{(1)} - A_2^{(2)} \cos \phi_2^{(2)}}$, [60]. Error bars are obtained from partitioning trajectories into two pieces. Grey error band is obtained as the standard deviation between separate series of measurements.

the order $m = 1$, i.e., the linear response, with convincing agreement. The phase angle for $m = 1$ is small for the frequencies measured, indicating that the force F_t is almost in phase with the protocol X_t , as for an elastic material. The black curve, extracted from equilibrium data, shows that with smaller ω the phase increases, presumably reaching $\pi/2$ in the limit of $\omega \rightarrow 0$. The slow increase with decreasing ω displays the slow nature of the investigated system.

The lower panel shows the phase for $m = 2$, i.e., to second order. While the agreement between the line and the data confirms Eq. (4), the graph shows that the difference of phases of first and second cumulants are rather small. In other words, first and second cumulants deviate noticeable in amplitude, seen in Fig. 2, but not so much in phase.

We presented and tested a non-equilibrium fluctuation identity for a driven classical system, emphasizing the validity on various length scales. Indeed, such relations are necessary, e.g., for a systematic coarse graining of non-equilibrium systems. The identity is confirmed for experiments of a Brownian particle interacting with a complex surrounding. Future work can explore other systems, aim at the next terms in Eq. (2), or investigate a possible quantum version.

This project was funded by the Deutsche Forschungsgemeinschaft (DFG), Grant No. SFB 1432 (Project ID 425217212)—Project C05.

* j.caspers@theorie.physik.uni-goettingen.de

† matthias.kruger@uni-goettingen.de

- [1] H. B. Callen and T. A. Welton, Phys. Rev. **83**, 34 (1951).
- [2] R. Kubo, Rep. Prog. Phys. **29**, 255 (1966).
- [3] L. D. Landau and E. M. Lifshitz, *Statistical Physics* (Pergamon, 1980).
- [4] A. G. Sitenko, *Electromagnetic Fluctuations In Plasma* (Academic Press, New York, 1967).
- [5] S. M. Rytov, I. A. Kravtsov, and V. Tatarskii, *Principles of Statistical Radiophysics* (Springer-Verlag, 1987).
- [6] J. P. Hansen and I. R. McDonald, *Theory of Simple Liquids: with Applications to Soft Matter* (Elsevier Science, 2013).
- [7] L. F. Cugliandolo, D. S. Dean, and J. Kurchan, Phys. Rev. Lett. **79**, 2168 (1997).
- [8] D. Ruelle, Phys. Lett. A **245**, 220 (1998).
- [9] A. Crisanti and F. Ritort, J. Phys. A: Math. Gen. **36**, R181 (2003).
- [10] T. Harada and S.-i. Sasa, Phys. Rev. Lett. **95**, 130602 (2005).
- [11] T. Speck and U. Seifert, EPL **74**, 391 (2006).
- [12] J. M. Deutsch and O. Narayan, Phys. Rev. E **74**, 026112 (2006).
- [13] R. Chetrite, G. Falkovich, and K. Gawedzki, J. Stat. Mech. **2008**, P08005 (2008).
- [14] U. M. B. Marconi, A. Puglisi, L. Rondoni, and A. Vulpiani, Phys. Rep. **461**, 111 (2008).

- [15] K. Saito, Europhys. Lett. **83**, 50006 (2008).
- [16] M. Baiesi, C. Maes, and B. Wynants, Phys. Rev. Lett. **103**, 010602 (2009).
- [17] J. Prost, J.-F. Joanny, and J. M. R. Parrondo, Phys. Rev. Lett. **103**, 090601 (2009).
- [18] T. Harada, Phys. Rev. E **79**, 030106 (2009).
- [19] M. Krüger and M. Fuchs, Phys. Rev. Lett. **102**, 135701 (2009).
- [20] U. Seifert and T. Speck, EPL **89**, 10007 (2010).
- [21] M. Baiesi, C. Maes, and B. Wynants, Proc. R. Soc. A: Math. Phys. Eng. Sci. **467**, 2792 (2011).
- [22] L. F. Cugliandolo, J. Phys. A: Math. Theor. **44**, 483001 (2011).
- [23] G. Verley, R. Chétrite, and D. Lacoste, J. Stat. Mech. **2011**, 10025 (2011).
- [24] B. Altaner, M. Poletini, and M. Esposito, Phys. Rev. Lett. **117**, 180601 (2016).
- [25] E. Lippiello, M. Baiesi, and A. Sarracino, Phys. Rev. Lett. **112**, 140602 (2014).
- [26] W. Wu and J. Wang, Front. Phys. **8** (2020).
- [27] L. Caprini, J. Stat. Mech. **2021**, 063202 (2021).
- [28] M. Baldovin, L. Caprini, A. Puglisi, A. Sarracino, and A. Vulpiani, in *Nonequilibrium Thermodynamics and Fluctuation Kinetics: Modern Trends and Open Questions* (Springer International Publishing, 2022).
- [29] M. K. Johnsrud and R. Golestanian, Generalized Fluctuation Dissipation Relations for Active Field Theories (2024), arXiv:2409.14977.
- [30] R. Kubo, J. Phys. Soc. Jpn. **12**, 570 (1957).
- [31] T. Yamada and K. Kawasaki, Prog. Theor. Phys. **38**, 1031 (1967).
- [32] D. J. Evans and G. Morriss, *Statistical Mechanics of Nonequilibrium Liquids*, 2nd ed. (Cambridge University Press, 2008).
- [33] M. Fuchs and M. E. Cates, J. Phys.: Condens. Matter **17**, S1681 (2005).
- [34] T. Holsten and M. Krüger, Phys. Rev. E **103**, 032116 (2021).
- [35] I. Oppenheim, Prog. Theor. Phys. Supp. **99**, 369 (1989).
- [36] J.-P. Bouchaud and G. Biroli, Phys. Rev. B **72**, 064204 (2005).
- [37] E. Lippiello, F. Corberi, A. Sarracino, and M. Zannetti, Phys. Rev. E **78**, 041120 (2008).
- [38] V. Lucarini and M. Colangeli, J. Stat. Mech. **2012**, P05013 (2012).
- [39] G. Diezemann, Phys. Rev. E **85**, 051502 (2012).
- [40] E. Wang and U. Heinz, Phys. Rev. D **66**, 025008 (2002).
- [41] D. Andrieux and P. Gaspard, J. Stat. Mech. **2007**, P02006 (2007).
- [42] M. Colangeli, C. Maes, and B. Wynants, J. Phys. A: Math. Theor. **44**, 095001 (2011).
- [43] U. Basu, M. Krüger, A. Lazarescu, and C. Maes, Phys. Chem. Chem. Phys. **17**, 6653 (2015).
- [44] U. Basu, L. Helden, and M. Krüger, Phys. Rev. Lett. **120**, 180604 (2018).
- [45] C. Maes, Front. Phys. **8** (2020).
- [46] J. Caspers and M. Krüger, J. Chem. Phys. **161**, 124109 (2024).
- [47] L. Helden, U. Basu, M. Krüger, and C. Bechinger, EPL **116**, 60003 (2016).
- [48] C. Maes, J. Stat. Phys. **154**, 705 (2014).
- [49] C. Maes, Phys. Rep. **850**, 1 (2020).
- [50] J. R. Gomez-Solano, A. Petrosyan, S. Ciliberto, R. Chétrite, and K. Gawedzki, Phys. Rev. Lett. **103**, 040601 (2009).
- [51] V. Blickle, T. Speck, C. Lutz, U. Seifert, and C. Bechinger, Phys. Rev. Lett. **98**, 210601 (2007).
- [52] J. Mehl, V. Blickle, U. Seifert, and C. Bechinger, Phys. Rev. E **82**, 032401 (2010).
- [53] J. R. Gomez-Solano, A. Petrosyan, S. Ciliberto, and C. Maes, J. Stat. Mech. **2011**, P01008 (2011).
- [54] J. Caspers and M. Krüger, tba (2025), Note: In the accompanying manuscript, x_t (not X_t) denotes the position of the control parameter at time t . The notation chosen here allows easier presentation.
- [55] C. Maes, SciPost Phys. Lect. Notes , 32 (2021).
- [56] The expansion in Eq. (2) suggests the dimensionless expansion parameter $\beta F \int_{t-\tau}^t ds \dot{x}_s$ with cumulant relaxation time τ .
- [57] M. E. Cates and S. J. Candau, J. Phys.: Condens. Matter **2**, 6869 (1990).
- [58] J. R. Gomez-Solano and C. Bechinger, New J. Phys. **17**, 103032 (2015).
- [59] ω is determined from the power spectral density, thus carrying an error depending on the length of the measurement.
- [60] As the phases $\phi_2^{(1)}$ and $\phi_2^{(2)}$ may differ, the coefficient ΔA_2 of the difference of first and second cumulants is found via $\Delta A_2 \equiv \sqrt{\left(A_2^{(1)}\right)^2 + \left(A_2^{(2)}\right)^2 - 2A_2^{(1)}A_2^{(2)} \cos\left(\phi_2^{(1)} - \phi_2^{(2)}\right)}$.